
This is the **accepted version** of the journal article:

Aguiló, Joan; Francàs Forcada, Laia; Bofill Arasa, Roger; [et al.]. «Powerful Bis-facially Pyrazolate-Bridged Dinuclear Ruthenium Epoxidation Catalyst». *Inorganic Chemistry*, Vol. 54, issue 14 (2015), p. 6782-6791. DOI 10.1021/acs.inorgchem.5b00641

This version is available at <https://ddd.uab.cat/record/288398>

under the terms of the  **IN COPYRIGHT** license

A Powerful Bis-facially Pyrazolate-Bridged Dinuclear Ruthenium Epoxidation Catalyst

Joan Aguiló,^{a,b} Laia Francàs,^b Roger Bofill,^a Marcos Gil-Sepulcre,^a Jordi García-Antón,^{a,c} Albert Poater,^d Antoni Llobet,^{a,b} Lluís Escriche,^{a*} Franc Meyer,^e and Xavier Sala^{a*}

^a Departament de Química, Facultat de Ciències, Universitat Autònoma de Barcelona, Cerdanyola del Vallès, 08193 Barcelona (Spain).

^b Institute of Chemical Research of Catalonia (ICIQ), Av. Països Catalans 16, 43007 Tarragona (Spain).

^c Serra Hünter Fellow.

^d Institut de Química Computacional i Catàlisi and Departament de Química, Universitat de Girona, Campus de Montilivi, 17071 Girona (Spain).

^e Institut für Anorganische Chemie, Georg-August-Universität, Tammannstrasse 4, 37077 Göttingen (Germany).

KEYWORDS: pyrazolate ligand, epoxidation catalysis, ruthenium catalyst, dinuclear catalyst, stereospecificity

ABSTRACT: A new bis-facial dinuclear ruthenium complex, $\{[\text{Ru}^{\text{II}}(\text{bpy})]_2(\mu\text{-bimp})(\mu\text{-Cl})\}^{2+}$, **2**²⁺, containing a hexadentate pyrazolate-bridging ligand (Hbimp) and bpy as auxiliary ligands has been synthesized and fully characterized in solution by spectrometric, spectroscopic and electrochemical techniques. The new compound has been tested with regard to its capacity to oxidize water and alkenes. The *in situ* generated bis-aqua complex, $\{[\text{Ru}^{\text{II}}(\text{bpy})(\text{H}_2\text{O})]_2(\mu\text{-bimp})\}^{3+}$, **3**³⁺, is an excellent catalyst for the epoxidation of a wide range of alkenes. High turnover numbers (TN), up to 1900, and turnover frequencies (TOF), up to 73 min⁻¹, are achieved using PhIO as oxidant. Moreover, **3**³⁺ presents an outstanding stereospecificity for both *cis* and *trans* olefins towards the formation of their corresponding epoxides due to specific interactions transmitted by its ligand scaffold. A mechanistic analysis of the epoxidation process has been performed based on DFT calculations in order to better understand the putative cooperative effects within this dinuclear catalyst.

The epoxidation of olefins, a process of great industrial and economical importance, has historically constituted a great challenge for the organic synthetic chemists.^{1,2} Epoxides constitute a family of essential chemicals, particularly for the synthesis of various polymers (polyglycols, polyamides, polyurethanes, etc.),^{3,4} and fine chemicals such as pharmaceuticals, food additives or flavor and fragrance compounds.⁵ For instance, propylene oxide monopolizes the epoxide chemical business with a yearly 8 million ton production and an expected annual increase of 5%.⁶

Enantioselective epoxidation of olefins and allylic alcohols is a chemical process of utmost industrial relevance. Numerous works by the Nobel laureate K.B. Sharpless with the Ti tartrate catalyst^{7,8} or by H. Jacobsen with Mn^{III}-salen catalysts^{9,10} have been proven efficient in this field. Thus, the Ti-tartrate catalyst consistently affords high enantioselectivities for widely different substrates thanks to a combination of stereoelectronic and steric factors, which leads to a concerted formation of both epoxide C-O bonds.⁸ Concerning the Mn^{III}-(salen) catalysts, enantioselectivity is provoked by the presence of a chiral diimine bridge and of bulky groups at the 3,3'-positions of the salen ligand and the existence of π conjugation of the olefinic double bond.⁹ In this case, epoxidation occurs by the direct attack of one of the C atoms of the C=C bond on the oxo ligand of a Mn(V)=O intermediate, generating a triplet radical species that would then collapse before or after rotating, thus

generating the *cis* or the *trans* epoxide, respectively, depending on the relative height of the activation barriers for collapse and rotation.¹⁰

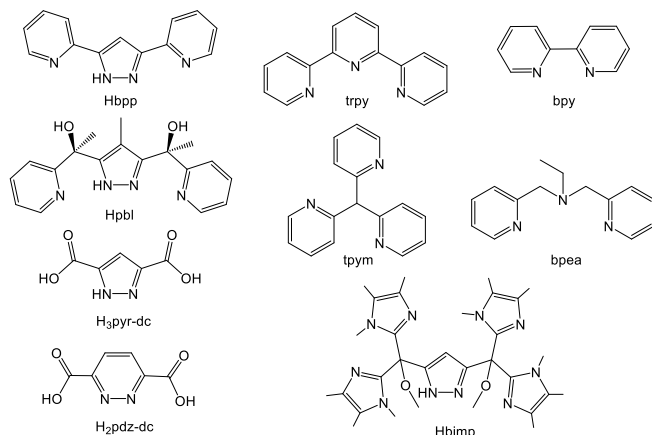
Ru complexes have also been proven to serve as excellent catalysts for redox transformations such as alcohol oxidation,¹¹⁻¹⁸ sulfoxidation,¹⁹⁻²² water oxidation²³⁻³² and epoxidation.^{18,33-41} In all these cases, a Ru^{IV}=O or Ru^V=O group has been shown to be the active catalytic unit. Most of the literature related to redox catalysis using Ru complexes is based on mononuclear complexes, since they are generally easily accessible from a synthetic point of view. In sharp contrast, two powerful diruthenium epoxidation catalysts in terms of epoxide selectivity and substrate conversion have been recently reported by our research group.^{42,43} In addition, these new catalysts display distinctive reactivity with regards to *cis* and *trans* alkenes. Both features are proposed to originate from a hydrogen bonding interaction between the second Ru^{IV}=O site and the substrate employed, together with steric effects.

Our groups have an extensive experience in the synthesis, characterization and evaluation of the oxidative catalytic performance of dinuclear Ru complexes, most of them inspired by the well-known $\{[\text{Ru}^{\text{II}}(\text{trpy})]_2(\mu\text{-bpp})(\mu\text{-Cl})\}^{2+}$ water oxidation catalyst.⁴⁴ Modifications around this paradigmatic compound, like the replacement of the trpy auxiliary ligands by facially coordinating scaffolds such as bpea or tpym, as well as the exchange of the bpp bridge by oth-

er tetradentate bridges as for instance pdz-dc²⁻, pyr-dc³⁻ or pbl (see Chart 1 for a drawing of these ligands) and by bis-meridional hexadentate bridges have been prepared, characterized and catalytically evaluated.^{42,43-48} The use of facial ligands such as bpea and tpym allowed an “up, down” relative orientation of the two Ru=O groups, which dramatically affects both the steric and electronic properties of these complexes as well as their final reactivity and water oxidation reaction mechanism.

The use of a bis-facial bridging ligand to prepare dinuclear Ru catalysts for water oxidation and/or olefin epoxidation has not been attempted so far. Therefore, in order to explore the properties of this kind of systems, herein we report the synthesis, spectroscopic and redox properties of a new dinuclear complex with formula {[Ru^{II}(bpy)]₂(μ-bimp)(μ-Cl)}²⁺, **2**²⁺, and its bis-aqua derivative {[Ru^{II}(bpy)(H₂O)]₂(μ-bimp)}³⁺, **3**³⁺ (bpy=2,2'-bipyridine; bimp=3,5-bis[bis(1,4,5-trimethylimidazol-2-yl)-methoxymethyl]pyrazolate). The already reported bimp-ligand⁴⁹ will act as bridging and bis-facial coordinating ligand. Finally, the reactivity of **3**³⁺ towards the epoxidation of olefins and a theoretical study on its putative epoxidation mechanism are reported in this work.

Chart 1. Bridging and auxiliary ligands discussed in this work.



RESULTS AND DISCUSSION

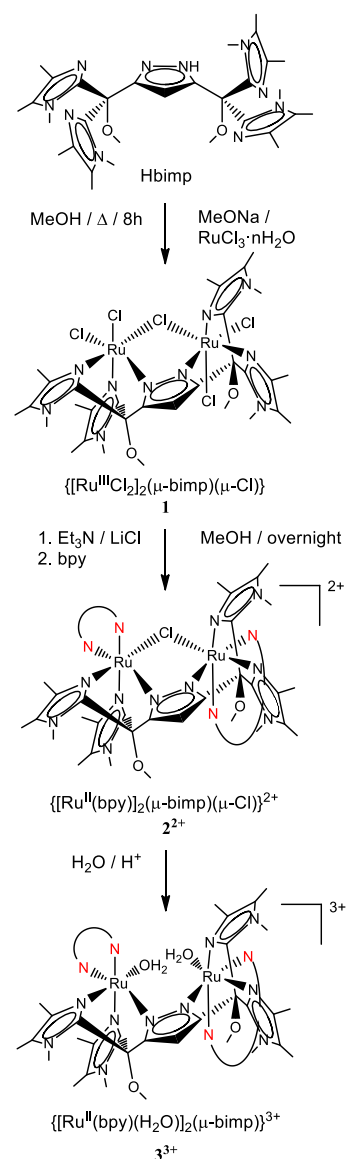
Synthesis and Structural Characterization of 2(PF₆)₂ and 3³⁺. The synthetic strategy followed for the preparation of the respective μ-chloro and bis-aqua dinuclear complexes **2(PF₆)₂** and **3³⁺** is depicted in Scheme 1.

Preparation of precursor **1** from RuCl₃·nH₂O involved the presence of sodium methoxide as a base to deprotonate the pyrazolic NH group of the Hbimp ligand. Because of the high solubility of **1** in the reaction media, the addition of diethyl ether was compulsory in order to precipitate the desired product as a green powder (see ESI-MS spectrum of **1** in Figure S1). The reaction of **1** in the presence of LiCl, triethylamine and 2,2'-bipyridine (2 equivalents) ended up generating **2**²⁺ after overnight stirring at room temperature. The addition of water and 1 mL of a saturated aque-

ous solution of NH₄PF₆ yielded a violet powder corresponding to the desired complex, **2(PF₆)₂**. The dissolution of **2(PF₆)₂** in a pH 1.0 aqueous solution (triflic acid 0.1 M) resulted in the generation of the bis-aqua complex **3³⁺**.

Each tridentate unit of the hexadentate μ-bimp⁻ ligand, given its configuration, can only coordinate in a facial fashion to an octahedral metal center. In addition, the μ-bimp⁻ ligand can potentially generate the C_s (*cis*) and C₂ (*trans*) isomers depicted in Figure 1. The terms *cis* and *trans* indicate whether the two bipyridines are located both on the same side (*cis*) or one above and one below (*trans*) of the distorted plane formed by the pyrazolate ring, the Ru metal centers and the chlorido bridge or the two coordinated aqua ligands.

Scheme 1. Synthetic pathway for the preparation of **2(PF₆)₂** and **3³⁺**. Bpy ligands have been represented schematically (red N atoms) for the sake of clarity.



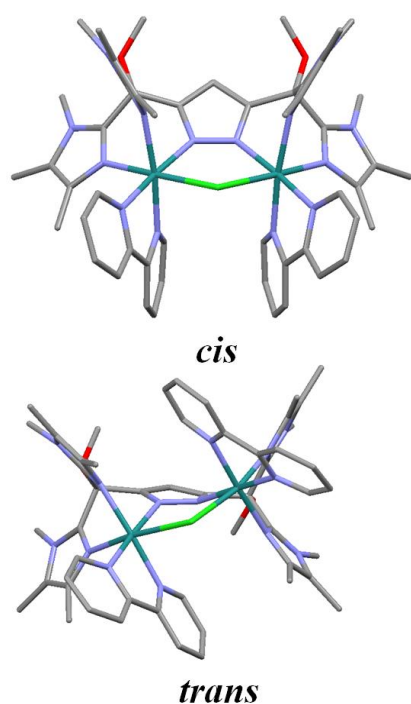


Figure 1. Mercury plot of the μ -Cl front view corresponding to the DFT calculated structures of *cis*- and *trans*- 2^{2+} . Atom color code: blue, nitrogen; light green, chlorine; dark green, ruthenium; light grey, carbon; red, oxygen; white, hydrogen. Hydrogen atoms have been omitted for clarity purposes.

Complex $2(\text{PF}_6)_2$ has been characterized in acetone solution by NMR spectroscopy (Figures 2 and S2) as well as by ESI-MS (Figure S4 in the Supporting Information).

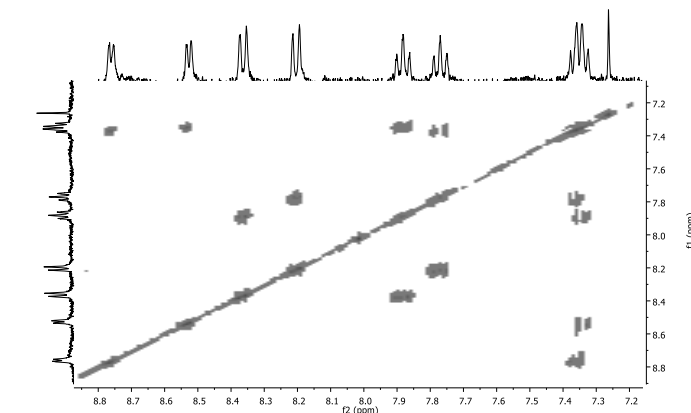
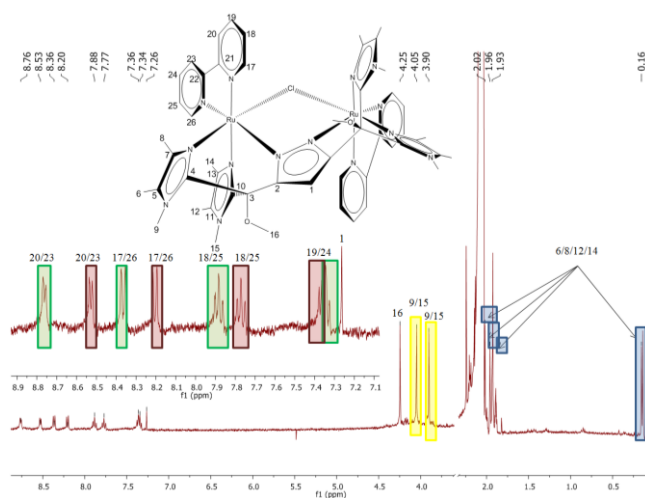


Figure 2. ^1H NMR spectra (400 MHz, 298 K, acetone- d_6) for 2^{2+} : 1D spectrum including partial assignment of signals (top) and 2D-COSY spectrum (bottom).

The broad ^1H NMR signals of 2^{2+} (Figure S2a) show the paramagnetic character of the sample, probably due to the partial oxidation of 2^{2+} . This oxidation is avoided under the presence of a reducing agent (Zn amalgam), when significantly narrower peaks are observed (Figure S2b). Figures 2 and S2c-e display both ^1H and ^{13}C $\{^1\text{H}\}$ 1D and 2D (COSY, HSQC and HMBC) NMR spectra for 2^{2+} . From these spectra, the presence of a single isomer of $2(\text{PF}_6)_2$ in solution could be deduced. However, the low solubility of the complex in the regular deuterated solvents and its above-mentioned ease of oxidation prevented the recording of a NOESY NMR spectrum. Therefore, the pyridine rings of each bpy and the four methyl groups bonded to the imidazole moieties could not be distinguished. For this reason, only a partial assignment of the ^1H (Figure 2, top) and ^{13}C resonances of 2^{2+} could be accomplished (see the Experimental Section).

DFT calculations have been carried out in order to further extract structural and electronic information about the potential *cis/trans* isomers. These calculations show for the chlorido-bridged complex 2^{2+} an energy value of 3.2 kcal/mol lower for the *trans* isomer compared to its *cis* counterpart (Figure 1 and Table S1). When the same calculations were carried out for the corresponding *cis* and *trans*-bis-aqua complex 3^{3+} (Figure 3 and Table S1), the *cis/trans* energy gap increased to 8.2 kcal/mol, again demonstrating the higher thermodynamic stability of the *trans* isomer. Even though these energy differences are not large enough to totally discard the formation of the *cis* isomer under the reaction conditions, they are a good indication of the potential formation of the *trans* compound given the isomeric purity of the obtained complex. Moreover, this hypothesis is further supported by the trends observed when performing a detailed comparison of the DFT-calculated structures for *cis*- and *trans*- 2^{2+} (Figure S3). Thus, for *cis*- 2^{2+} we observe the presence of repulsive $\text{H}\cdots\text{H}$ interactions among the methyl groups, between the methoxy and the CH group of the pyrazole ring, and among the CH groups of the bpps, together with the inexistence of π - π stacking interactions between the pyridine rings of neighboring bpps (torsion angle of 22.2°). In addi-

tion, significant tension within the *cis* complex exists, since the dihedral angle between the pyr rings of the same bpy is 27.0° and the Ru binding angles are far from ideal octahedral coordination. On the contrary, for *trans*-**2**²⁺ the repulsive H···H interactions are now abated (longer average H-H distances), while more favorable C···H interactions between the C atoms of the pyr rings and the H atoms of the methyl groups are observed (four interactions for the *trans* isomer compared to only one for the *cis* one). These data, together with a less tensioned conformation for the *trans* isomer (dihedral angle between pyr rings of the same bpy of only 16.3° and Ru binding angles a bit closer to ideal octahedral geometry), indicate a clear preference of **2**²⁺ for the *trans* configuration.

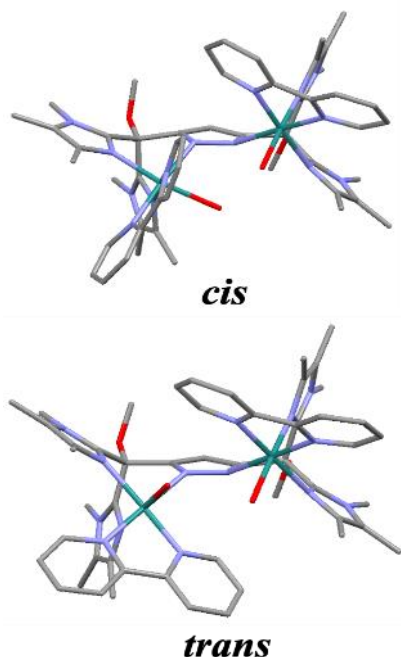
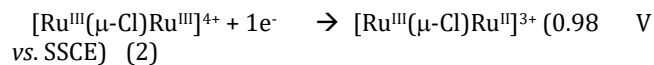
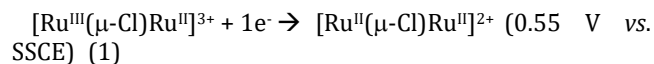


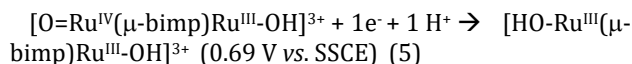
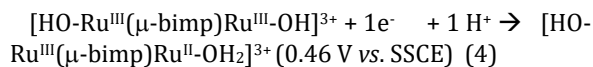
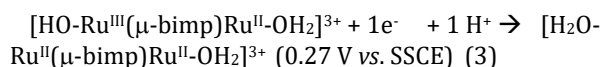
Figure 3. Mercury plot of the bis-H₂O front view corresponding to the DFT calculated structures of *cis*- and *trans*-**3**³⁺. Atom color code: blue, nitrogen; dark green, ruthenium; light grey, carbon; red, oxygen. Hydrogen atoms have been omitted for clarity purposes.

Electrochemical and Spectroscopic Characterization of **2²⁺ and **3**³⁺.** The CV of **2**²⁺ in DCM (Figure S5a) exhibits two reversible waves, also confirmed by DPV (Figure S5b), which can be assigned to the following electrochemical reactions (the bimp[−] and the bpy ligands are not shown for the sake of clarity):



The electrochemical properties of **3**³⁺ have been investigated after its “*in situ*” generation in an acetone:water (pH 1.0, 0.1 M triflic acid) 1:9 mixture by using **2**²⁺ as a precursor

(see Scheme 1 and the pH dependence of the DPV signals of the resulting complex in Figure S5c, which confirms the “*in situ*” formation of the bis-aqua complex **3**³⁺). From the CV and DPV (Figure 4) measurements of **3**³⁺, a total of four waves can be observed. The first three can be tentatively assigned, taking into account previous results on related complexes,²⁵ to the following redox processes:



When the potential is increased further up to 1.4 V, a large anodic current is observed in the DPV that is associated with an additional complex oxidation with a concomitant electrocatalytic oxidation of water to dioxygen. For the case of a further one electron oxidation, this would be in agreement with equations (6) and (7).

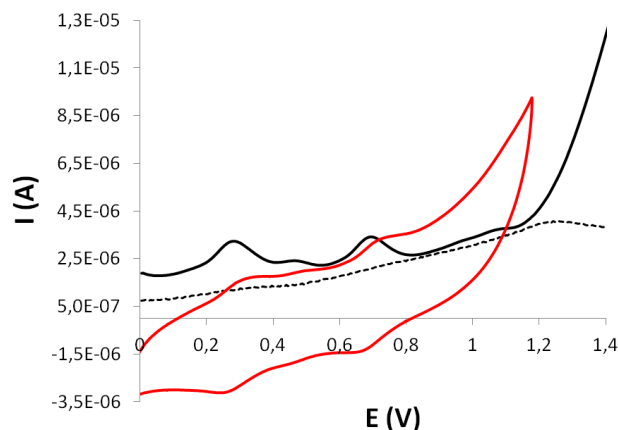
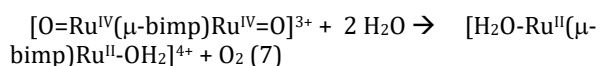
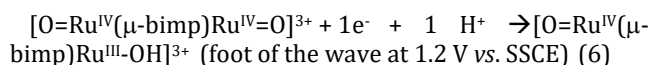


Figure 4. CV at 100 mV/s scan rate (red) and DPV (black) for the bis-aqua complex **3**³⁺ in acetone:water 1:9 pH 1.0 (0.1 M triflic acid). The DPV blank in the absence of catalyst is also shown (dashed line). A glassy carbon electrode was used as working electrode and the potential was measured vs. SSCE. For further details, see Experimental Section.

Table 1 displays the *E*_{1/2} values for **2**²⁺, **3**³⁺ and a set of related compounds containing the Hbpp ligand. The compounds have been classified depending on the σ-donor character of the coordinated N-donor ligand (pyridine < pyrazole ≈ imidazole < tertiary aliphatic amine) and the number of coordinated chlorido anions per Ru center (0 for the bis-aqua derivatives, ½ when a chlorido-bridge connects two Ru metal ions, or 1). Thus, a down-shift of *E*_{1/2} is observed when comparing **2**²⁺ with {[Ru^{II}(trpy)]₂(μ-bpp)(μ-Cl)}²⁺ (entry 2), in agreement with the higher σ-

donor and lower π -acceptor capacity of the imidazole rings relative to the pyridines that are part of the trpy ligand and also present in the Hbpp ligand. The redox potentials of 2^{2+} have also been compared to those of other bis-facial Ru dinuclear complexes (entries 3 and 4). With respect to the bpea complex (entry 3), both processes are anodically shifted by 180 and 260 mV, respectively, as a consequence of both the lower σ -donor and higher π -acceptor capacity of the imidazole rings in 2^{2+} relative to the central tertiary aliphatic amine in the bpea ligand and the lower σ -donation power of the unique chlorido-bridged anion of 2^{2+} in contrast to the two chlorido anions present in *trans*- $\{[Ru^{II}(bpea)(Cl)]_2(\mu-bpp)\}^+$. Interestingly, the redox potentials of 2^{2+} are similar to those of the tpym chlorido complex (entry 4). While in the latter each Ru is coordinated to 4 pyridines, 1 pyrazolato and one chlorido anion, in 2^{2+} each Ru is bound to 2 pyridines, 3 imidazole/pyrazolato rings and only half chlorido ligand. In consequence, the lower Cl⁻ content in 2^{2+} might compensate the more pronounced σ -donating character of its imidazole and pyrazole rings, thus revealing the influence of both the N-ligands and the chlorido anions into the final $E_{1/2}$ values, and how this property is a perfect combination of both factors.

Concerning the bis-aqua species, a cathodic shift of the $E_{1/2}$ values of 3^{3+} relative to those of *cis*- $\{[Ru^{II}(trpy)(H_2O)]_2(\mu-bpp)\}^{3+}$ and *trans*- $\{[Ru^{II}(tpym)(H_2O)]_2(\mu-bpp)\}^{3+}$ (entries 6 and 8) is observed, which can be explained again by the higher σ -donor and lower π -acceptor character of the imidazole rings compared to pyridines. Finally, similar $E_{1/2}$ values are observed for *trans*- $\{[Ru^{II}(bpea)(H_2O)]_2(\mu-bpp)\}^{3+}$ (entry 7) and 3^{3+} . Thus, the presence in the bpea complex of a strong σ -donor (aliphatic tertiary amine) and 3 pyridines results in similar average donor/acceptor properties than combining 2 imidazoles, 2 pyridines and one pyrazole in 3^{3+} .

The UV-vis spectra of 2^{2+} and 3^{3+} have been recorded in acetone and acetone:water 8:2 (pH 1), respectively (Figure S6). The region between 250 nm and 350 nm, usually displaying very intense bands due to the intraligand $\pi \rightarrow \pi^*$ transitions, could not be registered since it was out of the solvent window. With respect to the region between 350 nm and 550 nm, unsymmetrical broad metal-to-ligand charge transfer (MLCT) bands appear.^{50,51} For the chlorido-bridged complex 2^{2+} the MLCT bands are shifted to longer wavelengths due to the relative destabilization of the $d\pi(Ru)$ levels provoked by the chlorido ligand compared to the aqua ligands.

Table 1. Redox potentials in V (vs. SSCE) at a 100 mV/s scan rate for 2^{2+} , 3^{3+} and related Ru complexes.

Entr		III, II / II, II	III, III / III, II	IV, III / III, III	IV, IV / IV, III	N pyridine	N pyrazole / imidazole	N aliphatic amine	Cl	Ref.
1	$2^{2+ a}$	0.55	0.98	-	-	2	3	-	1/2	c
2	$\{[Ru^{II}(trpy)]_2(\mu-bpp)(\mu-Cl)\}^{2+ a}$	0.71	1.12	-	-	4	1	-	1/2	25
3	<i>trans</i> - $\{[Ru^{II}(bpea)(Cl)]_2(\mu-bpp)\}^{+ a}$	0.37	0.72	-	-	3	1	1	1	45
4	<i>trans</i> - $\{[Ru^{II}(tpym)(Cl)]_2(\mu-bpp)\}^{+ a}$	0.54	0.84	-	-	4	1	-	1	46
5	$3^{3+ b}$	0.27	0.46	0.69	1.20	2	3	-	-	c
6	<i>cis</i> - $\{[Ru^{II}(trpy)(H_2O)]_2(\mu-bpp)\}^{3+ b}$	0.59	0.65	0.88	1.10	4	1	-	-	25
7	<i>trans</i> - $\{[Ru^{II}(bpea)(H_2O)]_2(\mu-bpp)\}^{3+ b}$	0.21	0.43	0.61	-	3	1	1	-	45
8	<i>trans</i> - $\{[Ru^{II}(tpym)(H_2O)]_2(\mu-bpp)\}^{3+ b}$	0.54	0.75	1.18	1.52	4	1	-	-	46

^a CH₂Cl₂ using TBAPF₆ 0.1 M as electrolyte. ^b Aqueous solution at pH 1.0 (0.1 M triflic acid). ^c This work.

Epoxidation Catalysis. Complex 3^{3+} has been tested with regards to its ability to oxidize alkenes. The catalytic reactions have been carried out using a catalyst:substrate:oxidant:water ratio of 1:2000:4000:4000 after a 120 min mixing period of catalyst 2^{2+} in the absence of substrate (see Experimental Section for further details), during which the excess of water ensures the generation of the oxidant PhIO species from PhI(OAc)₂⁵² and of the bis-aqua derivative 3^{3+} from its chloro counterpart 2^{2+} . This mixing period before substrate addition is crucial in order to improve the rate of the catalytic reaction. Scheme S1 summarizes the set of reactions that take place during the catalytic epoxidation of alkenes for the proposed system. All products of each catalytic experiment have been identified by GC-MS (see Figures S7-S10 in the Supporting Information for further details).

The catalytic activity of 3^{3+} towards the epoxidation of alkenes has been initially tested and optimized for the oxidation of *cis*- β -methylstyrene, and its reaction progress monitored by GC and GC-MS. After that, six *cis*- and *trans*-olefins have been tested as substrates. All results from epoxidation catalysis are displayed in Table 2.

Table 2. Catalytic performance of **3**³⁺ in the epoxidation of *cis*- and *trans*-alkenes using PhIO as oxidant in DCE.^a

Entry	Alkene	Conv. (%) ^b	Selec. (%) ^c	TN/TOF _i ^d
1	<i>cis</i> - β -methylstyrene	>99	88	1760/73
2	<i>trans</i> - β -methylstyrene	50	80	800/21
3	<i>cis</i> -stilbene	>99	24	480/11
4	<i>trans</i> -stilbene	>99	14	280/4
5	<i>cis</i> -2-octene	95	100	1900/34
6	<i>trans</i> -2-octene	42	100	840/24
7	<i>cis</i> -2-hexene	93	100	1860/83
8	<i>trans</i> -2-hexene	58	100	1160/19
9	cyclooctene	95	65	1235/17

^a Catalyst:substrate:oxidant:water ratio of 1:2000:4000:4000. See Experimental Section for further procedural details. ^b Substrate conversion = $\{[\text{substrate}]_{\text{initial}} - [\text{substrate}]_{\text{final}}\} / [\text{substrate}]_{\text{initial}} \cdot 100$. ^c Epoxide selectivity = $[\text{epoxide}]_{\text{final}} / \{[\text{substrate}]_{\text{initial}} - [\text{substrate}]_{\text{final}}\} \cdot 100$. ^d TN is the turnover number with regard to the total epoxide obtained. TOF_i is the initial turnover frequency expressed in epoxide cycles per minute (TN_i/min).

The system **3**³⁺ 0.85 mM/*cis*- β -methylstyrene 1.7 M/PhI(OAc)₂ 3.4 M/H₂O 3.4 M in DCE renders 1.50 M *cis*- β -methylstyrene oxide, which represents a turnover number (TN) of 1760 with regard to the initial catalyst concentration after 90 minutes of reaction. The conversion of the initial substrate is total (>99%) after this time, and an epoxide selectivity of 88% is obtained. The activity of **3**³⁺ for the epoxidation of other alkenes is also very remarkable. For instance, the system **3**³⁺/*cis*-2-octene generates an impressive 1.62 M *cis*-2-octene oxide that represents a TN of 1900 with regard to the initial catalyst concentration, with an initial turnover frequency (TOF_i) of 34.0 cycles per minute.

Although the results herein reported are difficult to compare with those of related complexes from the literature due to the fact that catalysts and oxidants used are substantially different, some conclusions can be drawn. First, as a general trend, the reported Ru mononuclear species in the literature show lower epoxide selectivities and substrate conversions.^{53,54} And second, to our knowledge **3**³⁺ is more than 30 times faster than the best reported mononuclear Ru catalyst. Therefore, both figures suggest the existence of a potential cooperative effect between the two metal centers strategically situated in **3**³⁺ (see discussion below). Also, when comparing with our recently reported Ru dinuclear catalysts,^{42,43} **3**³⁺ performs better in the presence of aromatic *cis* substrates (*e.g.* higher conversion, selectivity and TN and TOF_i values for *cis*- β -methylstyrene compared to the pdz-dc⁴² and pyr-dc⁴³ counterparts, and for *cis*-stilbene higher conversion and TN figures com-

pared to both previous catalysts and an even higher TOF_i value than its pdz-dc counterpart⁴²).

A deeper look at Table 2 also shows that **3**³⁺ performs much better with substrates containing electron-donor groups than with those bearing electron-withdrawers. Thus, the best results are obtained for *cis*-2-octene and *cis*-2-hexene, whereas the poorest values are obtained for *trans*-stilbene, the latter also suffering from potential steric effects due to the bulkiness of its two phenyl rings. Also, the performance of **3**³⁺ in front of *cis*- and *trans*- β -methylstyrene, which could be seen as hybrids between the corresponding *cis*-/*trans*-stilbene and *cis*-/*trans*-2-octene/hexene substrates from a steric and electronic point of view, is indeed intermediate between the two extremes probably due to a combination of the two effects described above. Furthermore, the electronic effects are in agreement with the electrophilic character of the Ru^{IV}=O active site proposed in related works.^{42,43} Also, it is worth mentioning the lower activity and selectivity of the catalyst towards *trans* substrates with regard to their related *cis* counterparts (Table 2 and Figure 5, top). Given the nearly identical electronic nature of the *cis* and *trans* alkenes, the differential reactivity can only be due to distinctive interactions with the catalyst. To understand and rationalize the origin of this differentiated reactivity, we carried out DFT calculations of the energy and structure of the putative *cis*- and *trans*-O=Ru^{IV}-Ru^{IV}=O active species, which pointed to a higher thermodynamic stability for the *trans*-configuration (12.9 kcal/mol) compared to its *cis* counterpart (Figure 5, bottom, and Table S1). Knowing the potential structure of the catalytic active species, it is clear that the aforementioned interactions may be a consequence of the high steric constrictions imposed by the cavity of the catalyst around the Ru^{IV}=O active sites. Thus, selectivity in favor of the *cis* or *trans* isomer of the substrate is determined by the ability of the alkene isomers to better fit into the reactive pocket of the catalyst (Figure 5, bottom).

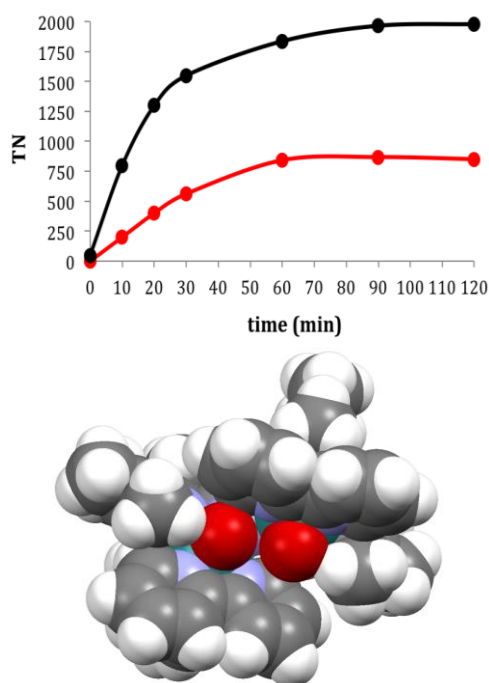
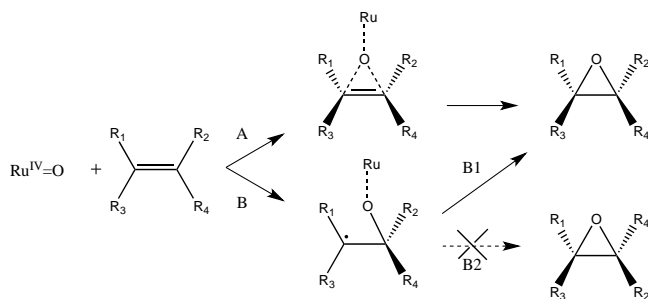


Figure 5. Top: evolution of *cis*- β -methylstyrene oxide (black line) and *trans*- β -methylstyrene oxide (red line) when employing 3^{3+} as catalyst (top). Bottom: Mercury spacefilling plot of the structure of the *trans*-O=Ru^{IV}-Ru^{IV}=O DFT-calculated state for catalyst 3^{3+} . Color code: oxygen, red; carbon, light grey; hydrogen, white; nitrogen, light blue; ruthenium, green.

Another interesting feature of the system studied in this work is the stereospecific nature of the catalytic process, since no *cis/trans* isomerization takes place for neither the *cis*- nor the *trans*-alkenes. This points out towards a mechanism of either a concerted oxygen atom transfer from the Ru^{IV}=O active site to the double bond of the alkene (path A, Scheme 2) or a radical pathway where the C-C rotation of the generated radical is much slower than the ring closing that generates the final epoxide (path B1, Scheme 2).⁵⁵⁻⁵⁹

Scheme 2. Proposed stereoselective (A, B1) and non-stereoselective (B2) mechanisms for the epoxidation of alkenes by Ru^{IV}=O species.



DFT calculations have been performed for 3^{3+} in the presence of *cis*- and *trans*- β -methylstyrene, *cis*- and *trans*-

stilbene, and *cis*- and *trans*-2-octene in order to quantify the energetics associated with the steric constraints that direct the epoxidation process (Figure S11 and Tables 3 and S1). The ground state multiplicity of all putative species was accurately evaluated, revealing that the initial bis-aqua species is a singlet, whereas the bis-oxo species is a quintuplet, and the presumed radical species present during the formation of the new C-O bond as well as the final epoxide species are triplets.

The results obtained show that the rate determining step (rds) of the whole process involves the interaction of the double bond of the alkene with one of the Ru=O groups that eventually will transfer the O-atom to the olefin (steps A or B, Scheme 2, and TS(A→B), Figure S11, and Tables 3 and S1). However, the interaction of a Ru=O group with both carbon atoms of the olefin in a concerted way is not feasible, and thus all attempts collapse in a mono O...C interaction. This radical pathway is analogous to the one proposed for the [Mn^{III}(salen)Cl] catalyst,¹⁰ and differs fundamentally from the mechanism proposed for the Ti tartrate catalyst, where both epoxide C-O bonds are formed simultaneously.⁸ Finally, the low stability of the radical species formed facilitates the formation of the final epoxide, except for the case of *cis*-2-octene, where its non-aromatic nature does probably not allow the localization of such radical intermediate, which could in turn be the reason why selectivity is as high as 100% (Table 2).

Interestingly, DFT calculations indicate that the transition state of this rds (TS(A→B)) is favored by 2.1, 0.9 and 5.6 kcal/mol for the *cis* isomer with respect to the *trans* substrate in the cases of β -methylstyrene, stilbene and 2-octene, respectively (Tables 3 and S1), which could be an explanation for the higher observed experimental rates (TOFi) for the *cis* substrates (Table 2).

Table 3. Relative energies in kcal/mol with respect to initial substrate and catalyst *trans*- 3^{3+} of the most stable epoxidation pathway of the *cis* and *trans* isomers of β -methylstyrene, stilbene and 2-octene.^a

	A	TS(A→B)	B	TS(B→C)	C
<i>cis</i> - β -methylstyrene	0.0	21.0	11.5	11.6	0.3
<i>trans</i> - β -methylstyrene	0.0	23.1	12.6	12.7	0.3
<i>cis</i> -stilbene	0.0	23.5	5.1	13.8	-1.3
<i>trans</i> -stilbene	0.0	24.4	8.9	17.8	8.5
<i>cis</i> -2-octene	0.0	23.6	--	--	-5.1
<i>trans</i> -2-octene	0.0	29.2	--	--	-0.8

^a A = *trans*- 3^{3+} + substrate, B = radical intermediate, C = epoxide product bound to *trans*- 3^{3+} .

Additionally, an analysis of the Ru=O...H distances lower than 3 Å in TS(A→B) for the reaction of *trans*- 3^{3+} with both *cis* and *trans* substrates (Figures S12-S14) shows that

while for *trans*- β -methylstyrene three different H interactions between the oxo groups and the substrate exist (O1-CH, O1-CH₃, O2-CH₃; being O1 the epoxy-forming atom and O2 the second oxo group, not involved in O transfer), for *cis*- β -methylstyrene an additional O1-CH₃ interaction happens (Figure S12). Analogously, for *trans*-stilbene three different H interactions between the oxo groups and the substrate exist (O1-CH_{arom}, O1-CH_{olefinic}, O2-CH_{olefinic}; being O1 the epoxy-forming atom and O2 the second oxo group), while for *cis*-stilbene an additional O2-CH interaction happens (there are two O1-CH_{olefinic} interactions plus an O2-CH_{olefinic} and an O2-CH_{arom} interaction, Figure S13). In the two previous cases, those differences can only arise from the dissimilar orientation of the C=C bond as well as the different configuration of the *cis* vs. *trans* substrates, thus demonstrating the more favored TS(A→B) for the substrate in *cis* configuration, which in turn may be in accordance with the lower calculated TS(A→B) energies (Table 3) and the higher experimental conversion, TN and TOF, values (Table 2) reported above. At the same time, this could also explain the better performance of 3³⁺ in front of aromatic *cis* substrates compared to its pdz-dc⁴² and pyrdc⁴³ counterparts. Concerning 2-octene, no clear differences among the Ru=O...H distances arise between the *cis* and *trans* substrate (four interactions of an average 2.5 Å distance, Figure S14), although since in this case no clear mechanism has been envisaged by DFT calculations (attempts to detect states B and TS(B→C) have been unsuccessful, Tables 3 and S1), the explanation of the observed reactivity differences between the *cis* and *trans* substrate may not be as straightforward as in the two previous cases.

In short, in TS(A→B) the catalyst interacts with the substrate through the second Ru=O group, provoking intermolecular H-bond interactions with the aliphatic and/or aromatic substituents of the alkene. The latter phenomenon may be crucial for dictating the stereoselectivity of the catalyst. This second Ru=O group is situated in the cavity shown in Figure 5 (bottom), and in consequence the degree of interaction with a particular substrate will depend on the synergistic effect of combining the accommodation capacity of the substrate (steric effects) within the cavity with the substrate capacity to generate H-interactions with this second Ru=O group. This synergy between both Ru=O groups may also be the responsible for the observed higher epoxidation rates and selectivities of 3³⁺ compared to the already reported Ru mononuclear epoxidation catalysts.⁶⁰

Conclusions. The *in situ* generated bis-aqua, bis-facial Ru dinuclear complex 3³⁺ containing the hexadentate pyrazolate-bridging ligand bimp⁻ is a catalyst with an impressive performance towards the epoxidation of a wide range of olefins. From the scope of the analyzed substrates, the following results can be pointed out: a) *cis*-alkenes are epoxidized faster and in higher yields than their corresponding *trans* counterparts; b) substrates containing electron-donor groups yield better results than those bearing electron-withdrawers -because of the highly electrophilic character of the Ru^{IV}=O active sites-; and c) the catalytic system is stereospecific in nature, *i.e.*, no *cis/trans*

isomerization takes place. We have also shown that a radical pathway where the C-C rotation of the generated radical is slower than the ring closing that generates the final epoxide is the likely mechanism for this transformation, at least for the cases of β -methylstyrene and stilbene. Also, the dinuclear complex 3³⁺ in the form *trans*-O=Ru^{IV}-Ru^{IV}=O behaves stereoselectively probably due to the different role of each of the two Ru=O groups. While the first one is responsible for oxygen transfer, the second one appears to be involved in H interactions. The latter may also be influenced by the ligand architecture of the catalyst, thus generating a discriminating pocket for the incoming substrates. The combination of these factors renders 3³⁺ one of the few examples of powerful stereoselective epoxidation catalysts that do not need the use of substrates with specific modifications.

EXPERIMENTAL SECTION

Materials. All reagents used in the present work were obtained from Aldrich Chemical Co. and were used without further purification. Reagent-grade organic solvents were obtained from Scharlab. RuCl₃·3H₂O was supplied by Alfa Aesar and was used as received. Synthesis and characterization of Hbimp ligand are reported in the literature.⁴⁹ All synthetic manipulations were routinely performed under nitrogen atmosphere using Schlenk tubes and vacuum-line techniques.

Instrumentation and Measurements. UV-Vis spectroscopy was performed by a HP8453 spectrometer using 1 cm quartz cells. NMR spectroscopy was performed on a Bruker DPX 250 MHz, DPX 360 MHz or a DPX 400 MHz spectrometer. Samples were run in CDCl₃, CD₃CN or acetone-d₆ with internal references. Electrospray ionization mass spectrometry (ESI-MS) experiments were carried out on an HP298s gas chromatography (GC-MS) system from the Servei d'Anàlisi Química de the Universitat Autònoma de Barcelona (SAQ-UAB). Cyclic voltammetry (CV) and differential pulse voltammetry (DPV) experiments were performed on an Ij-Cambria HI-660 potentiostat using a three-electrode cell. A glassy carbon electrode (2 mm diameter) was used as working electrode, platinum wire as auxiliary electrode and a SSCE as a reference electrode. Working electrodes were polished with 0.05 micron Alumina paste washed with distilled water and acetone before each measurement. The complexes were dissolved in acetone, DCM or acetone:water 1:9 containing the necessary amount of *n*-Bu₄NPF₆ (TBAPF₆) for the purely organic solvent cases or triflic acid pH 1.0 for the latter as supporting electrolyte to yield 0.1 M ionic strength solution. CV were recorded at a 100 mV·s⁻¹ scan rate, and DPV were recorded using pulse amplitudes of 0.05 V, pulse widths of 0.05 s, sampling widths of 0.02 s, pulse periods of 0.1 s and quite times of 2 s. *E*_{1/2} values reported in this work were estimated from CV experiments as the average of the oxidative and reductive peak potentials (*E*_{p,a} + *E*_{p,c})/2. Epoxidation catalytic experiments were performed as follows. First, a mixing period of 120 min was carried out by adding in a vial 1 mL of 1,2-dichloroethane (DCE) as

solvent, 1.60 g (5.0 mmol) of (diacetoxyiodo)benzene ($\text{PhI}(\text{OAc})_2$) as oxidant, 1 mmol of dodecane as internal standard, 1.8 mg ($1.25 \cdot 10^{-3}$ mmol) of catalyst **2**⁺, and 90 μL (5.0 mmol) of water. This mixing period before substrate addition was observed to be key in order to improve the rate of the catalytic reaction. Then, the substrate (2.5 mmol) was added to the previous mixture, thus achieving a final volume of approx. 1.47 mL and the corresponding initial concentrations: catalyst, 0.85 mM; substrate, 1.7 M; dodecane, 0.68 M; $\text{PhI}(\text{OAc})_2$, 3.4 M; water, 3.4 M. These concentrations correspond to a catalyst:substrate:oxidant:water ratio of 1:2000:4000:4000. Aliquots were taken every 5, 10, 15, 20, 25 or 30 min until completion of reaction. Each aliquot was filtered through a Pasteur pipette filled with celite; after that diethyl ether was added in order to elute the organic compounds and the filtrate was analyzed in an Agilent 6890N gas chromatograph (GC) coupled to a mass selective detector with ionization by electronic impact, or in an Agilent 6890 GC with a flame ionization detector (FID) detector using a HP5 column. The characterization of the reaction products were done by comparison with commercial products or by GC-MS spectrometry. GC conditions: initial temperature 40 °C for 10 min, ramp rate variable for each substrate (typically from 10 °C/min to 20 °/min), final temperature 250 °C, injection temperature 220 °C, detector temperature 250 °C. Yield of epoxide and substrate conversion were calculated with regard to the initial concentration of substrate.

Substrate conversion = $\frac{[\text{substrate}]_{\text{initial}} - [\text{substrate}]_{\text{final}}}{[\text{substrate}]_{\text{initial}}} \cdot 100$. Epoxide selectivity = $\frac{[\text{epoxide}]_{\text{final}}}{[\text{substrate}]_{\text{initial}} - [\text{substrate}]_{\text{final}}} \cdot 100$.

Computational Details. Density functional theory (DFT) calculations have been carried out with the Gaussian 09 set of programs,⁶¹ using the BP86 functional of Becke and Perdew.⁶²⁻⁶⁴ The electronic configuration of the molecular systems was described with the standard split-valence basis set with a polarization function of Ahlrichs and co-workers for H, C, N, O, and Cl (SVP keyword in Gaussian).⁶⁵ For Ru we used the small-core, quasi-relativistic Stuttgart/Dresden effective core potential, with an associated valence basis set contracted (standard SDD keywords in Gaussian 09).⁶⁶⁻⁶⁸ The geometry optimizations were performed without symmetry constraints, and the characterization of the located stationary points was performed by analytical frequency calculations.

The reported energies include solvent effects estimated with the polarizable continuous solvation model PCM,^{69,70} using DCE as a solvent, calculated through single point energy calculations on the BP86 geometries with using the M06L functional⁷¹ and the 6-311+G(d,p) basis set^{72,73} for main group atoms.

Overall, the relative Gibbs energies reported in this work include energies computed using the M06L/6-311+G(d,p)//BP86/SVP method together with solvent effects obtained at the M06L/6-311+G(d,p) level, and zero-point energies, thermal corrections and entropy effects calculated at 298 K with the BP86/SVP method.

Synthetic preparations. $\{[\text{Ru}^{\text{III}}\text{Cl}_2]_2(\mu\text{-bimp})(\mu\text{-Cl})\}$ [**1**]. A sample of Hbimp (0.382 mmol) was dissolved in 40 mL of dry methanol, then 1.8 mL of 0.2108 M MeONa (0.382 mmol) were added. The mixture was stirred at RT during 10 minutes, and 200 mg (0.765 mmol) of $\text{RuCl}_3 \cdot 3\text{H}_2\text{O}$ were added. The resulting solution was heated at reflux overnight while vigorous magnetic stirring was maintained. After this time the volume was reduced in the rotary evaporator and diethyl ether was added. The resulting solid was filtered and washed with diethyl ether. Yield: 336 mg (91%). ESI-MS (MeOH): $m/z = 926.1$ ($[\text{M} - 2\text{Cl} + \text{MeO}]^+$). Elemental analysis calcd for $\text{C}_{31}\text{H}_{43}\text{Cl}_5\text{N}_{10}\text{O}_2\text{Ru}_2$: C, 38.51; H, 4.49; N, 14.50. Found: C, 38.62; H, 4.50; N, 14.39.

$\{[\text{Ru}^{\text{II}}(\text{bpy})]_2(\mu\text{-bimp})(\mu\text{-Cl})(\text{PF}_6)_2$ [**2**](PF_6)₂]. A mixture of 300 mg (0.311 mmol) of complex **1**, 39 mg (0.933) of LiCl and 172.5 μL (1.244 mmol) of NEt_3 were dissolved in 90 mL of dry methanol. The mixture was stirred during 30 min and then 96 mg (0.622 mmol) of bpy were added. The resulting solution was overnight stirred at RT. After this time the crude was filtered and 3 mL of NH_4PF_6 saturated aqueous solution and 30 mL of water were added to the filtrate. The volume was reduced until a violet precipitate appeared, which was filtered and washed with cold diethyl ether. Yield: 200 mg (45%). ^1H NMR (400 MHz, $[\text{D}_6]\text{acetone}$): $\delta = 8.76$ (d, 2H, $J = 5.20$ Hz, H20 or H23), 8.53 (d, 2H, $J = 5.20$ Hz, H20 or H23), 8.36 (d, 2H, $J = 7.30$ Hz, H17 or H26), 8.20 (d, 2H, $J = 7.30$ Hz, H17 or H26), 7.88 (t, 2H, $J = 8.90$ Hz, $J = 7.75$ Hz, H18 or H25), 7.77 (t, 2H, $J = 8.90$ Hz, $J = 7.75$ Hz, H18 or H25), 7.36 (t, 2H, H19 or H24), 7.34 (t, 2H, H19 or H24), 7.26 (s, 1H, H1), 4.25 (s, 3H, H16), 4.05 (s, 3H, H9 or H15), 3.90 (s, 3H, H9 or H15), 2.02, 1.96, 1.93, 0.16. $^{13}\text{C}\{^1\text{H}\}$ NMR (100 MHz, $[\text{D}_6]\text{acetone}$): $\delta = 161.57$ (C21/22), 161.07 (C21/22), 157.32 (C20/23), 156.51 (C20/23), 154.86 (C2), 145.41 (C4/10), 143.32 (C4/10), 137.37 (C7/13), 136.06 (C7/13), 135.60, (C18/25), 134.53 (C18/25), 128.47 (C5/11), 126.66 (C19/24), 125.80 (C5/11), 124.30 (C17/24), 124.07 (C19/24), 122.88 (C17/24), 106.28 (C1), 85.35 (C3), 57.03 (C16), 33.05 (C9/15), 32.83 (C9/15), 13.62, 9.13, 8.67, 8.51. ESI-MS (MeOH): $m/z = 1283.2$ ($[\text{M} - \text{PF}_6]^+$). Elemental analysis calcd for $\text{C}_{51}\text{H}_{59}\text{ClF}_{12}\text{N}_{14}\text{O}_2\text{P}_2\text{Ru}_2$: C, 42.85; H, 4.16; N, 13.73. Found: C, 42.83; H, 4.20; N, 13.67.

ASSOCIATED CONTENT

Supporting Information. Additional spectroscopic, spectrometric, electrochemical and computational (DFT) data. This material is available free of charge via the Internet at <http://pubs.acs.org>.

AUTHOR INFORMATION

Corresponding Author

- Fax: + 34 93 581 24 77 E-mail: luis.escriche@uab.cat, xavier.sala@uab.cat
- Homepage: www.seloecat.wordpress.com

Notes

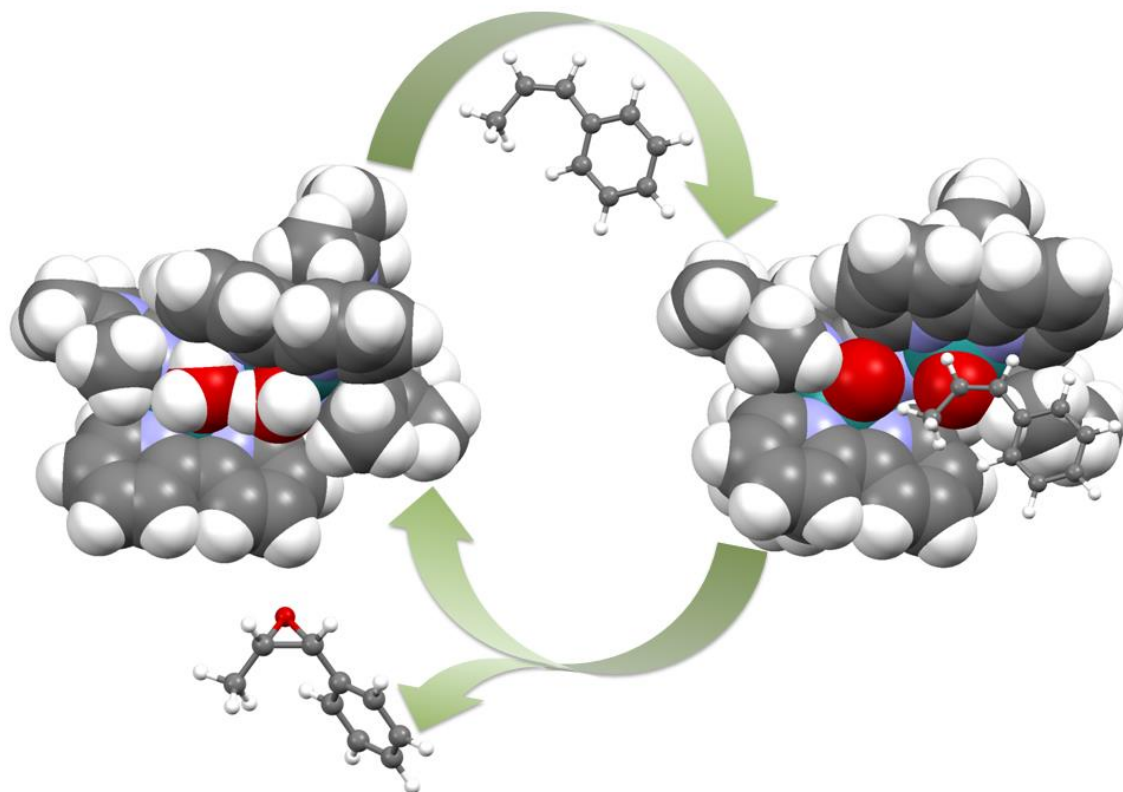
The authors declare no competing financial interest.

ACKNOWLEDGMENT

• Support from MINECO (CTQ2011-26440, CTQ 2010-21497 and CTQ2010-21532-C02-02) and the DFG (Me1313/9-1) is gratefully acknowledged. J.A. is grateful for the award of a PIF doctoral grant from UAB. A.P. thanks the Spanish MINECO for a Ramón y Cajal contract (RYC-2009-05226) and the European Commission for a Career Integration Grant (CIG09-GA-2011-293900).

ABBREVIATIONS

Bpy, 2,2'-bipyridine; CV, Cyclic Voltammetry; DCE, 1,2-dichloroethane; DCM, Dichloromethane; DPV, Differential Pulse Voltammetry; DFT, Density Functional Theory; GC, Gas Chromatography; MS, Mass Spectrometry; Pyr, pyridine; rds, rate determining step; RT, Room Temperature; TN, Turnover Number; TOF, Turnover Frequency; TS, Transition State



A novel Ru(II) dinuclear complex containing the bis-facial hexadentate bridging ligand Hbimp is described. This complex is an excellent catalyst for the epoxidation of a wide range of alkenes, yielding high turnover numbers and turnover frequencies. Furthermore, an outstanding stereospecificity for both *cis* and *trans* olefins towards the formation of the corresponding epoxides is envisaged due to cooperative effects transferred by the Hbimp scaffold.

REFERENCES

- (1) Sheldon, R. A. *J. Mol. Catal.* **1980**, *7*, 107-126.
- (2) Joergensen, K. A. *Chem. Rev.* **1989**, *89*, 431-458.
- (3) Cavani, F.; Teles, J. H. *ChemSusChem* **2009**, *2*, 508-534.
- (4) Crivello, J. V. *J. Polym. Sci. Part A: Polym. Chem.* **2014**, *52*, 2934-2946.
- (5) Roberts, S. M.; Whittall, J., Eds., *Catalysts for fine chemical synthesis: Regio- and stereo-controlled oxidations and reductions*, Vol. 5; John Wiley Sons, Ltd: England, 2007.
- (6) Nijhuis, T. A.; Makkee, M.; Moulijn, J. A.; Weckhuysen, B. M. *Ind. Eng. Chem. Res.* **2006**, *45*, 3447-3459.
- (7) Woodard, S. S.; Finn, M. G.; Sharpless, K. B. *J. Am. Chem. Soc.* **1991**, *113*, 106-113.
- (8) Finn, M. G.; Sharpless, K. B. *J. Am. Chem. Soc.* **1991**, *113*, 113-126.
- (9) Jacobsen, H.; Cavallo, L. *Chem. Eur. J.* **2001**, *7*, 800-807.
- (10) Cavallo, L.; Jacobsen, H. *Angew. Chem. Int. Ed.* **2000**, *39*, 589-592.
- (11) Bäckvall J.-E.; Chowdhury, R. L.; Karlsson, U. *J. Chem. Soc., Chem. Commun.* **1991**, 473-475.
- (12) Wang, G.-Z.; Andreasson, U.; Bäckvall, J.-E. *J. Chem. Soc., Chem. Commun.* **1994**, 1037-1038.
- (13) Murahashi, S.I.; Naota, T. *Adv. Met.-Org. Chem.* **1994**, *3*, 225-253.
- (14) Murahashi, S.-I.; Naota, T. *Zh. Org. Khim.* **1996**, *32*, 223-232.
- (15) Friedrich, H. B. *Platinum Met. Rev.* **1999**, *43*, 94-102.
- (16) Keene, F. R. *Coord. Chem. Rev.* **1999**, *187*, 121-149.
- (17) Csajernyik, G.; Éll, A. H.; Fadini, L.; Pugin, B.; Bäckvall, J.-E. *J. Org. Chem.* **2002**, *67*, 1657-1662.
- (18) Murahashi, S.-I., Ed.; *Ruthenium in Organic Synthesis*, Wiley-VCH: Weinheim, Germany, 2004.
- (19) Mlodnicka, T.; James, B. R. *Catal. Met. Complexes* **1994**, *17*, 121-148.
- (20) Huynh, M. H. V.; Witham, L. M.; Lasker, J. M.; Wetzler, M.; Mort, B.; Jameson, D. L.; White, P. S.; Takeuchi, K. J. *J. Am. Chem. Soc.* **2003**, *125*, 308-309.
- (21) Hamelin, O.; Ménage, S.; Charnay, F.; Chavarot, M.; Pierre, J.-L.; Pécaut, J.; Fontecave, M. *Inorg. Chem.* **2008**, *47*, 6413-6420.
- (22) Benet-Buchholz, J.; Comba, P.; Llobet, A.; Roeser, S.; Vadivelu, P.; Wiesner, S. *Dalton Trans.* **2010**, *39*, 3315-3320.
- (23) Gersten, S. W.; Samuels, G. J.; Meyer, T. J. *J. Am. Chem. Soc.* **1982**, *104*, 4029-4030.
- (24) Gilbert, J. A.; Eggleston, D. S.; Murphy, Jr., W. R.; Geselowitz, D. A.; Gersten, S. W.; Hodgson, D. J.; Meyer, T. J. *J. Am. Chem. Soc.* **1985**, *107*, 3855-3864.
- (25) Sens, C.; Romero, I.; Rodríguez, M.; Llobet, A.; Parella, T.; Benet-Buchholz, J. *J. Am. Chem. Soc.* **2004**, *126*, 7798-7799.
- (26) Zong, R.; Thummel, R. P. *J. Am. Chem. Soc.* **2005**, *127*, 12802.
- (27) Tseng, H.-W.; Zong, R.; Muckerman, J. T.; Thummel, R. *Inorg. Chem.* **2008**, *47*, 11763-11773.
- (28) Concepcion, J. J.; Jurss, J. W.; Templeton, J. L.; Meyer, T. J. *J. Am. Chem. Soc.* **2008**, *130*, 16462-16463.
- (29) Sala, X.; Romero, I.; Rodríguez, M.; Escriche, L.; Llobet, A. *Angew. Chem., Int. Ed.* **2009**, *48*, 2842-2852.
- (30) Xu, Y.; Åkermark, T.; Gyollai, V.; Zou, D.; Eriksson, L.; Duan, L.; Zhang, R.; Åkermark, B.; Sun, L. *Inorg. Chem.* **2009**, *48*, 2717-2719.
- (31) Xu, Y.; Fischer, A.; Duan, L.; Tong, L.; Gabrielsson, E.; Åkermark, B.; Sun, L. *Angew. Chem., Int. Ed.* **2010**, *49*, 8934-8937.
- (32) Duan, L.; Bozoglian, F.; Mandal, S.; Stewart, B.; Privalov, T.; Llobet, A.; Sun, L. *Nat. Chem.* **2012**, *4*, 418-423.
- (33) Groves, J. T.; Quinn, R. *J. Am. Chem. Soc.* **1985**, *107*, 5790-5792.
- (34) Bailey, C. L.; Drago, R. S. *J. Chem. Soc., Chem. Commun.* **1987**, 179-180.
- (35) Stultz, L. K.; Binstead, R. A.; Reynolds, M. S.; Meyer, T. J. *J. Am. Chem. Soc.* **1995**, *117*, 2520-2532.
- (36) Barf, G. A.; Sheldon, R. A. *J. Mol. Catal. A.* **1995**, *102*, 23-39.
- (37) Porter, M. J.; Skidmore, J. J. *J. Chem. Soc., Chem. Commun.* **2000**, 1215-1225.
- (38) Arends, I. W. C. E.; Kodama, T.; Sheldon, R. A. *Top. Organomet. Chem.* **2004**, *11*, 277-320.
- (39) Bhor, S.; Tse, M. K.; Klawonn, M.; Doeblner, C.; Maegerlein, W.; Beller, M. *Adv. Synth. Catal.* **2004**, *346*, 263-267.
- (40) Bäckvall, J.-E., Ed., *Modern Oxidation Methods*, 2nd completely revised ed.; Wiley-VCH Verlag GmbH & Co. KGaA: Weinheim, Germany, 2010.
- (41) Serrano, I.; López, M. I.; Ferrer, I.; Poater, A.; Parella, T.; Fontrodona, X.; Solà, M.; Llobet, A.; Rodríguez, M.; Romero, I. *Inorg. Chem.* **2011**, *50*, 6044-6054.
- (42) Di Giovanni, C.; Vaquer, L.; Sala, X.; Benet-Buchholz, J.; Llobet, A. *Inorg. Chem.* **2013**, *52*, 4335-4345.
- (43) Di Giovanni, C.; Poater, A.; Benet-Buchholz, J.; Cavallo, L.; Solà, M.; Llobet, A. *Chem. Eur. J.* **2014**, *20*, 3898-3902.
- (44) García-Antón, J.; Bofill, R.; Escriche, L.; Llobet, A.; Sala, X. *Eur. J. Inorg. Chem.* **2012**, *30*, 4775-4789.
- (45) Mola, J.; Dinioi, C.; Sala, X.; Rodríguez, M.; Romero, I.; Parella, T.; Fontrodona, X.; Llobet, A. *Dalton Trans.* **2011**, *40*, 3640-3646.
- (46) Maji, S.; Vigara, L.; Cottone, F.; Bozoglian, F.; Benet-Buchholz, J.; Llobet, A. *Angew. Chem., Int. Ed.* **2012**, *124*, 6069-6072.
- (47) Neudeck, S.; Maji, S.; López, I.; Meyer, S.; Meyer, F.; Llobet, A. *J. Am. Chem. Soc.* **2014**, *136*, 24-27.
- (48) Sander, A. C.; Maji, S.; Francàs, L.; Böhnisch, T.; Dechert, S.; Llobet, A.; Meyer, F. *ChemSusChem* **2015**, <http://dx.doi.org/10.1002/cssc.201403344>.
- (49) Müller, H.; Bauer-Siebenlist, B.; Csapo, E.; Dechert, S.; Farkas, E.; Meyer, F. *Inorg. Chem.* **2008**, *47*, 5278-5292.
- (50) Takeuchi, K.J.; Thompson, M.S.; Pipes, D.W.; Meyer, T. J. *Inorg. Chem.* **1984**, *23*, 1845-1851.
- (51) Rodríguez, M.; Romero, I.; Llobet, A. *Inorg. Chem.* **2001**, *40*, 4150-4156.
- (52) In, J.-H.; Park, S.-E.; Song, R.; Nam, W. *Inorg. Chim. Acta* **2003**, *343*, 373-376.
- (53) Sala, X.; Santana, N.; Serrano, I.; Plantalech, E.; Romero, I.; Rodríguez, M.; Llobet, A.; Jansat, S.; Gómez, M.; Fontrodona, X. *Eur. J. Inorg. Chem.* **2007**, 5207-5214.
- (54) Serrano, I.; Sala, X.; Plantalech, E.; Rodríguez, M.; Romero, I.; Jansat, S.; Gómez, M.; Parella, T.; Stoeckli-Evans, H.; Solans, X.; Font-Bardia, M.; Vidjayacoumar, B.; Llobet, A. *Inorg. Chem.* **2007**, *46*, 5381-5389.
- (55) Srinivasan, K.; Michaud, P.; Kochi, J. K. *J. Am. Chem. Soc.* **1986**, *108*, 2309-2320.
- (56) Zona, T. A.; Goodman, J. L. *J. Am. Chem. Soc.* **1995**, *117*, 5879-5880.
- (57) Baciocchi, E.; Boschi, T.; Cassioli, L.; Galli, C.; Jaquinod, L.; Lapi, A.; Paolesse, R.; Smith, K. M.; Tagliatesta, P. *Eur. J. Org. Chem.* **1999**, 3281-3286.
- (58) Muray, E.; Illa, O.; Castillo, J. A.; Alvarez-Larena, A.; Bourdelande, J. L.; Branchadell, V.; Ortuno, R. M. *J. Org. Chem.* **2003**, *68*, 4906-4911.
- (59) Kumar, D.; de Visser, S. P.; Shaik, S. *Chem. Eur. J.* **2005**, *11*, 2825-2835.

-
- (60) Di Giovanni, C.; Poater, A.; Benet-Buchholz, J.; Cavallo, L.; Solà, M.; Llobet, A. *Chem. Eur. J.* **2014**, *20*, 3898-3902.
- (61) *Gaussian 09, Revision A.1*, Frisch, M. J.; Trucks, G. W.; Schlegel, H. B.; Scuseria, G. E.; Robb, M. A.; Cheeseman, J. R.; Scalmani, G.; Barone, V.; Mennucci, B.; Petersson, G. A.; Nakatsuji, H.; Caricato, M.; Li, X.; Hratchian, H. P.; Izmaylov, A. F.; Bloino, J.; Zheng, G.; Sonnenberg, J. L.; Hada, M.; Ehara, M.; Toyota, K.; Fukuda, R.; Hasegawa, J.; Ishida, M.; Nakajima, T.; Honda, Y.; Kitao, O.; Nakai, H.; Vreven, T.; Montgomery, Jr., J. A.; Peralta, J. E.; Ogliaro, F.; Bearpark, M.; Heyd, J. J.; Brothers, E.; Kudin, K. N.; Staroverov, V. N.; Kobayashi, R.; Normand, J.; Raghavachari, K.; Rendell, A.; Burant, J. C.; Iyengar, S. S.; Tomasi, J.; Cossi, M.; Rega, N.; Millam, J. M.; Klene, M.; Knox, J. E.; Cross, J. B.; Bakken, V.; Adamo, C.; Jaramillo, J.; Gomperts, R.; Stratmann, R. E.; Yazyev, O.; Austin, A. J.; Cammi, R.; Pomelli, C.; Ochterski, J. W.; Martin, R. L.; Morokuma, K.; Zakrzewski, V. G.; Voth, G. A.; Salvador, P.; Dannenberg, J. J.; Dapprich, S.; Daniels, A. D.; Farkas, Ö.; Foresman, J. B.; Ortiz, J. V.; Cioslowski, J.; Fox, D. J. Gaussian, Inc., Wallingford CT, **2009**.
- (62) Becke, A. *Phys. Rev. A* **1988**, *38*, 3098-3100.
- (63) Perdew, J. P. *Phys. Rev. B* **1986**, *33*, 8822-8824.
- (64) Perdew, J. P. *Phys. Rev. B* **1986**, *34*, 7406-7406.
- (65) Schaefer, A.; Horn, H.; Ahlrichs, R. *J. Chem. Phys.* **1992**, *97*, 2571-2577.
- (66) Haeusermann, U.; Dolg, M.; Stoll, H.; Preuss, H. *Mol. Phys.* **1993**, *78*, 1211-1224.
- (67) Kuechle, W.; Dolg, M.; Stoll, H.; Preuss, H. *J. Chem. Phys.* **1994**, *100*, 7535-7542.
- (68) Leininger, T.; Nicklass, A.; Stoll, H.; Dolg, M.; Schwerdtfeger, P. *J. Chem. Phys.* **1996**, *105*, 1052-1059.
- (69) Barone, V.; Cossi, M. *J. Phys. Chem. A* **1998**, *102*, 1995-2001.
- (70) Tomasi, J.; Persico, M. *Chem. Rev.* **1994**, *94*, 2027-2094.
- (71) Zhao, Y.; Truhlar, D. G. *J. Chem. Phys.* **2006**, *125*, 194101.
- (72) Hehre, W. J.; Ditchfield, R.; Pople, J. A. *J. Chem. Phys.* **1972**, *56*, 2257-2261.
- (73) Hariharan, P. C.; Pople, J. A. *Theor. Chim. Acta* **1973**, *28*, 213-222.